Pergamon

Int. J. Multiphase Flow Vol. 20, No. 1, pp. 45–61, 1994

0301-9322/94 $6.00 + 0.00

LIMIT CONDITIONS OF STEADY-STATE COUNTERCURRENT ANNULAR FLOW AND THE ONSET OF FLOODING, WITH REFERENCE TO THE CHF OF BOILING IN A BOTTOM-CLOSED VERTICAL TUBE

Y. KATTO

Department of Mechanical Engineering, Nihon University, Kanda-Surugadai, Chiyoda-ku, Tokyo 101, Japan

(Received 9 April 1993; in revised form 8 August 1993)

Abstract—An analytical study on the limit conditions of steady-state countercurrent annular flow in a vertical tube has been performed, aiming at the prediction of the onset of flooding in tubes where it is difficult for unstable wave motion to occur. A new expedient method is developed to determine the limit conditions under the involved flow conditions. It is revealed that the limit conditions in this flow system appear only when the interfacial shear stress increases with the liquid film thickness. A prediction model that takes the full effects of the void fraction ϵ into account, and a simplified model that considers only the effect of the liquid film thickness on the interfacial shear stress under a fixed condition of $\epsilon = 1$ are dealt with, showing that they predict the experimental data fairly well at low liquid flow rates, and that the latter model performs better than the former one. Finally, there is a brief discussion as to the possibility of the application of the present analysis to the prediction of the critical heat flux of boiling in a bottom-closed vertical tube.

Key Words: flooding, countercurrent annular flow, thermosyphon

1. INTRODUCTION

A large number of studies on flooding have been performed to date; and Imura *et al.* (1977), Tien & Liu (1979), McQuillan & Whalley (1985), Bankoff & Lee (1986) and others have surveyed the studied and data correlations. The majority of the studies assume that flooding is caused by some kind of wave motion or instability which occurrs on the gas/liquid interface, together with the entrainment of liquid droplets.

There are, however, a small number of models, such as those employed by Wallis (1969, p. 343), Bharathan *et al.* (1979), Bharathan & Wallis (1983) and Lee & Bankoff (1983), which consider the limit for the existence of the steady-state countercurrent two-phase flow as the condition to initiate flooding. Namely, if there is an equation governing the above-mentioned two-phase flow—$F(j_G^*, j_L^*, \epsilon) = 0$, where j_G^* and j_L^* are the Wallis dimensionless superficial velocities of the gas and liquid phase and ϵ is the void fraction—it gives flow curves of constant void fraction, such as those represented in figure 1, where the dimensionless liquid film thickness δ/R, R is the tube radius, is used in place of the void fraction ϵ for convenience. Then, an envelope generated by these curves can be determined mathematically by solving the following simultaneous equations with two unknowns j_G^* and j_L^*:

$$F(j_G^*, j_L^*, \epsilon) = 0 \quad G(j_G^*, j_L^*, \epsilon) = \frac{\partial F}{\partial \epsilon} = 0, \qquad [1]$$

where the second equation is the derivative of the first equation with respect to ϵ. In deriving the first equation of [1], Wallis (1969, p. 343) employed a drift-flux model, while the other two studies, Bharathan *et al.* (1979) and Lee & Bankoff (1983), assumed separated-flow models with friction at the gas/liquid interface. (*Note:* Richter (1981), Taitel *et al.* (1982) and Maron & Dukler (1984) also reported analyses based on the liquid film flow, but their criterion for the onset of flooding are different from the concept of the envelope given by [1]).

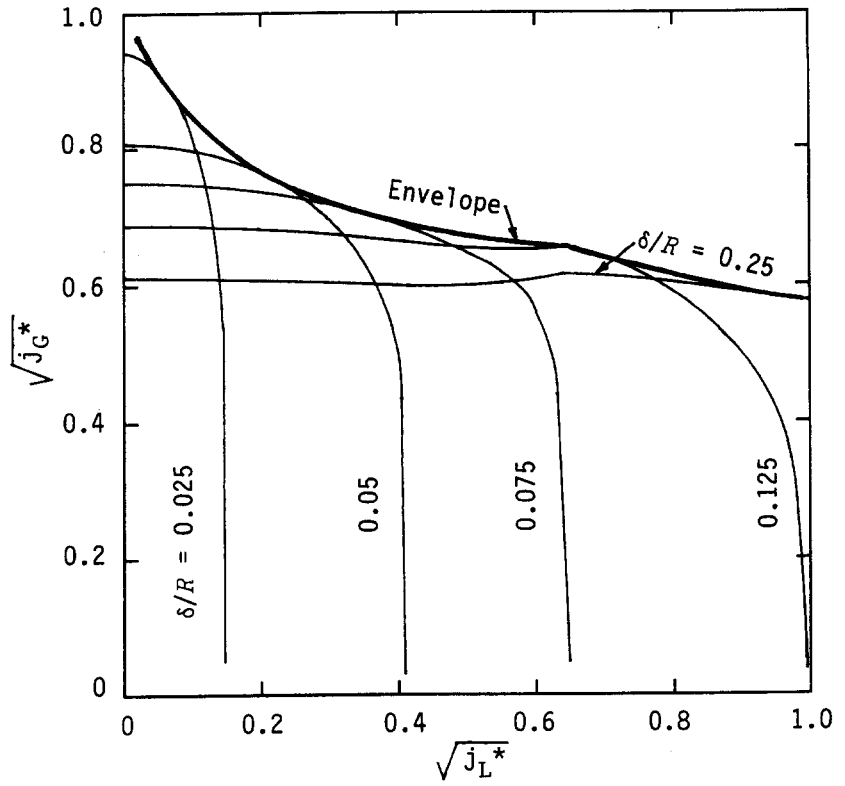

Figure 1. An envelope generated with flow curves of constant δ/R (air–water, 101.3 kPa, 20°C, $D = 20$ mm).

Meanwhile, Dobran (1985) and Reed & Tien (1987) performed analytical studies relating to the transient characteristics of two-phase closed thermosyphons. They employed lumped models based on equations of continuity, momentum and energy with interfacial friction between the two phases. A common liquid film thickness was assumed by Dobran (1985) throughout the three sections of the condenser, adiabatic and evaporator, while Reed & Tien (1987) assumed an individual mean liquid film thickness at each of the three sections. Then, Katto & Watanabe (1992) and Katto (1992) analyzed the limit conditions of steady-state countercurrent annular flow with interfacial friction, assuming a continuous change in the liquid film thickness along the tube wall. Their studies relate to the critical heat flux (CHF) of boiling in a vertical tube and an annulus with a saturated-liquid plenum at the top and a closed bottom end.

In conventional experiments of flooding, liquid is supplied to a vertical tube from the top and gas is supplied from the bottom end. In other words, each phase holds a constant mass flow rate throughout the tube and, hence, generally flooding can take place depending on the critical conditions which may appear at various parts of the tube. However, if one considers experiments such as those with a vertical tube with a special structure to avoid the interaction between the gas and liquid flow at the bottom end, the cause of flooding may be simplified. Similarly, in the case of saturated boiling in a bottom-closed vertical tube, boiling liquid generates vapor flow, and hence the mass flow rates of the liquid and vapor are equal at any cross section, taking the highest value at the top end. In other words, the limit condition of such a boiling system is localized at the top end of the tube, and hence the influence of other parts of the tube may be diminished.

Consequently, there is a possibility that an analysis of flooding based on the concept of the limit of steady-state countercurrent annular flow is particularly useful for such special flow systems. A study is made in this paper to consolidate the basis of the above-mentioned limit analysis, including the development of a new method which avoids the difficulty created by the use of the second of equations [1] under complicated conditions.

2. GOVERNING EQUATIONS AND CALCULATION PROCEDURE

For a countercurrent two-phase flow in a vertical tube, the governing equations are derived on the basis of a separated-flow model consisting of an upward core gas flow and a downward liquid film flow along the tube wall. In addition, it is assumed for the sake of simplicity that the individual states of the liquid and gas flow can be determined by their respective Reynolds numbers, and that the friction and pressure of the core gas flow are transmitted to the liquid film flow through the interface on the premise that the liquid film flow is comparatively thin.

2.1. The case of laminar liquid film flow

For laminar liquid film flow along the tube wall, the following equation of motion holds:

$$\mu_L \frac{\partial}{\partial r}\left(r\frac{\partial u}{\partial r}\right) + r\zeta = 0, \qquad [2]$$

where μ_L is the dynamic viscosity of the liquid, r is the radial coordinate, u is the downward velocity and ζ appears as

$$\zeta = \rho_L g - \frac{dp}{dx} \quad \text{and} \quad \frac{dp}{dx} = \frac{2\tau_i}{R-\delta} + \rho_G g.$$

In the first of the above two expressions, ρ_L, g and dp/dx are the liquid density, the gravitational acceleration and the pressure gradient (x is the the downard coordinate), respectively. The right-hand expression is an equation derived from the force balance of the core gas flow, where τ_i is the shear stress on the interface, R is the tube radius, δ is the liquid film thickness and ρ_G is the gas density. Combining these two expressions gives

$$\zeta = \rho_L g\left[\left(1-\frac{\rho_G}{\rho_L}\right) - \frac{2\tau_i}{\rho_L g R\left(1-\frac{\delta}{R}\right)}\right]. \qquad [3]$$

Now, integrating [2], and considering $\mu_L(\partial u/\partial r) = \tau_i$ at $r = R-\delta$ and $u = 0$ at $r = R$, gives the velocity distribution $u(r)$. With this $u(r)$, the mass flow rate of the liquid film per unit tube perimeter Γ can be evaluated by

$$2\pi R\Gamma = 2\pi\rho_L \int_{R-\delta}^{R} ru\, dr, \qquad [4]$$

leading to the result:

$$\frac{1}{4}\left(1-\frac{\delta}{R}\right)^4 \ln\frac{1}{1-\frac{\delta}{R}} - \frac{1}{16}\frac{\delta}{R}\left(2-\frac{\delta}{R}\right)\left[2-6\frac{\delta}{R}+3\left(\frac{\delta}{R}\right)^2\right]$$
$$= \frac{\Gamma\mu_L}{\rho_L\zeta R^3} + \frac{\tau_i}{\zeta R}\left(1-\frac{\delta}{R}\right)\left[\frac{1}{4}\frac{\delta}{R}\left(2-\frac{\delta}{R}\right) - \frac{1}{2}\left(1-\frac{\delta}{R}\right)^2 \ln\frac{1}{1-\frac{\delta}{R}}\right]. \qquad [5]$$

Expanding both sides of [5] with respect to δ/R and neglecting terms smaller than $(\delta/R)^2$, leads to the following relationship:

$$\frac{\delta}{R} = \frac{\frac{3\Gamma\mu_L}{\rho_L\zeta\delta^2 R} + \frac{3\tau_i}{2\zeta R}\left[1-\frac{4}{3}\left(\frac{\delta}{R}\right)+\frac{1}{4}\left(\frac{\delta}{R}\right)^2\right]}{1-\frac{\delta}{R}-\frac{3}{20}\left(\frac{\delta}{R}\right)^2}, \qquad [6]$$

where ζ is given by [3]. In this paper, the analysis will be limited to within the range of $\delta/R < 0.25$ (or more strictly, $\delta/R < 0.15$).

2.2. The case of turbulent film flow

For turbulent liquid film flow, a similar analysis to the preceding section is possible by assuming the Karman velocity distribution, for example. However, the accuracy of this method is not so good

when applied to a liquid film flow and, besides, it requires three complicated formulas. Hence, a simple method is adopted here; i.e. if the shear stress caused by the tube wall on the liquid flow is denoted by τ_w, the following expression generally holds from the force balance of the liquid film flow:

$$\frac{\delta}{R} = \frac{\tau_w + \left(1 - \frac{\delta}{R}\right)\tau_i}{R\left(1 - \frac{\delta}{2R}\right)\zeta}, \qquad [7]$$

where τ_w is evaluated by the equation of Wallis (1969, p. 329) for turbulent liquid film flow,

$$\tau_w = \tfrac{1}{2}\rho_L u_L^2 C_{fw} \qquad [8]$$

where

$$C_{fw} = 0.079\left(\frac{1}{\mathrm{Re}_{LF}^{1/4}}\right)$$

is the wall friction coefficient and Re_{LF} is the film Reynolds number. As for ζ on the right-hand side of [7], it can be evaluated by [3], because [3] holds universally and is independent of the flow state.

2.3. Reynolds number of the core gas and the liquid film flow

When the mass flow rates of the gas and liquid are m_G and m_L, respectively, the mean velocity of the core gas flow u_G (positive in the upward direction) and that of the liquid film flow u_L (positive in the downward direction) are

$$u_G = \frac{m_G}{\rho_G \pi (R-\delta)^2} = \frac{m_G}{\rho_G \pi R^2 \left(1 - \frac{\delta}{R}\right)^2} \qquad [9]$$

and

$$u_L = \frac{m_L}{\rho_L \pi [R^2 - (R-\delta)^2]} = \frac{m_L}{\rho_L 2\pi R\delta\left(1 - \frac{\delta}{2R}\right)}. \qquad [10]$$

Then, the relatively velocity u' between the gas and the liquid and the core gas Reynolds number Re'_G are defined, respectively, as follows:

$$u' = u_g + u_L \qquad [11]$$

and

$$\mathrm{Re}'_G = \frac{u'(2R - 2\delta)}{\nu_G} = \frac{u' 2R}{\nu_G}\left(1 - \frac{\delta}{R}\right), \qquad [12]$$

where ν_G is the kinematic viscosity of the gas. The mass flow rate of the liquid film per unit tube perimeter Γ and the film Reynolds number Re_{LF} are written, respectively, as follows:

$$\Gamma = \frac{m_L}{2\pi R} \qquad [13]$$

and

$$\mathrm{Re}_{LF} = \frac{4\Gamma}{\mu_L}. \qquad [14]$$

2.4. Evaluation of τ_i in [3], [6] and [7]

The shear stress at the interface τ_i is evaluated by

$$\tau_i = \tfrac{1}{2}\rho_G (u')^2 C_{fi}, \qquad [15]$$

where u' is the relative velocity between the liquid velocity at the interface and the mean velocity of the core gas flow and C_{fi} is the interfacial friction coefficient.

The definition of u' is somewhat different between [11] and [15]. However, the magnitude of the

interfacial liquid velocity u_{Li} is of the same order as u_L within the conditions of the present study, while u_L is extremely low compared with u_G. Consequently, $|u_{Li} - u_L| \ll u_G$ and, hence, u' of [11] can be used for u' in [15] without serious error.

The interfacial friction coefficient C_{fi} in [15] is evaluated by the following equations:

for laminar core gas flow,

$$C_{fi} = \frac{16}{Re'_G}; \qquad [16]$$

and

for turbulent core gas flow,

$$C_{fi} = 0.005 + x_1\left(\frac{\delta}{R}\right)^{x_2}. \qquad [17]$$

x_1 and x_2 are functions of the Bond number $Bo = (4\rho_L g R^2/\sigma)^{1/2}$ only, as

$$x_1 = 0.2574\left(\frac{Bo}{2}\right)^{x_2} 10^{9.07/Bo}$$

and

$$x_2 = 1.63 + \frac{4.74}{Bo}.$$

Equation [17] is an empirical correlation obtained by Bharathan *et al.* (1979) following the interfacial-roughness concept for the pressure drop in annular flow originated by Wallis (1970); and [17] has recently been used widely by Bharathan & Wallis (1983), Lee & Bankoff (1983), Dobran (1985), Reed & Tien (1987) and Katto & Watanabe (1992).

Next, if the core gas flow is in the transition region, the magnitude of C_{fi} is calculated by the following relationships, based on a two-step linear approximation of C_{fi} in the transition region (Katto & Watanabe 1992):

for $2900 < Re'_G < 11{,}000$,

$$\frac{C_{fi} - C_{fi[16]}}{0.8C_{fi[17]} - C_{fi[16]}} = \frac{Re'_G - 2900}{11{,}000 - 2900};$$

and

for $11{,}000 < Re'_G < 20{,}000$,

$$\frac{C_{fi} - 0.8C_{fi[17]}}{C_{fi[17]} - 0.8C_{fi[17]}} = \frac{Re'_G - 11{,}000}{20{,}000 - 11{,}000}. \qquad [18]$$

Where $C_{fi[16]}$ is the value of C_{fi} of [16] at $Re'_G = 2900$ and $C_{fi[17]}$ is the value of C_{fi} of [17], i.e. independent of Re'_G.

2.5. Calculation procedure

Equation [6] or [7] can be expressed in a unified form as

$$Y_1 = Y_2, \qquad [19]$$

where $Y_1 = \delta/R$, while Y_2 designates the right-hand side of [6] or that of [7] depending on the state of the liquid film flow (see table 1). Then, if values of j_G^*, j_L^* and $\delta/R\ (= Y_1)$ are assumed, Re'_G and Re_{LF} can be evaluated by [12] and [14], respectively. Through these Reynolds numbers, the flow states of the gas and liquid phase are known, and then Y_2 of [19] can be computed by employing the right-hand side of [6] or [7], where τ_i is evaluated by [15]. Finally, if the magnitude of Y_2 thus calculated satisfies [19], then the initially assumed values of j_G^*, j_L^* and δ/R are the flow situation satisfying [19].

In table 1, part (A) represents the foregoing calculation procedure systematically, where the states of the gas and liquid flow are subdivided into three characteristic regions. When the liquid film

Table 1(A, B). Equations used to compute Y_2 of [19] for given values of j_G^*, j_L^* and δ/R $(=Y_1)$

(A) The ϵ Model			
State of core gas flow Re'_G: [9]–[12]	Laminar ($Re'_G < 2900$)	Transition ($2900 < Re'_G < 20{,}000$)	Turbulent ($20{,}000 < Re'_G$)
Evaluation of τ_i	τ_i: [15] where C_{fi}: [16]	τ_i: [15] where C_{fi}: [18]	τ_i: [15] where C_{fi}: [17]
State of liquid film flow Re_{LF}: [13, 14]	Laminar ($Re_{LF} < 2040$)	Transition ($2040 < Re_{LF} < 3500$)	Turbulent ($3500 < Re_{LF}$)
Computation of Y_2	Y_2: RHS of [6] where ζ: [3]	Y_2: [20] where $Y_{2,lam}$: RHS of [6] $Y_{2,tur}$: RHS of [7]	Y_2: RHS of [7] where ζ: [3] τ_w: [8]
(B) The Non-ϵ Model			
State of core gas flow Re'_G: [22, 11]	Laminar ($Re'_G < 2900$)	Transition ($2900 < Re'_G < 20{,}000$)	Turbulent ($20{,}000 < Re'_G$)
Evaluation of τ_i	τ_i: [15] where C_{fi}: [16]	τ_i: [15] where C_{fi}: [18]	τ_i: [15] where C_{fi}: [17]
State of liquid film flow Re_{LF}: [13, 14]	Laminar ($Re_{LF} < 2040$)	Transition ($2040 < Re_{LF} < 3500$)	Turbulent ($3500 < Re_{LF}$)
Computation of Y_2	Y_2: RHS of [21]	Y_2: [19] where $Y_{2,lam}$: RHS of [21] $Y_{2,tur}$: RHS of [22]	Y_2: RHS of [22] where τ_w: [8]

flow is in the transition region, the evaluation of τ_w included in [7] is complicated. Hence, based on the idea of Reed & Tien (1987), Y_2 is evaluated by

$$Y_2 = \frac{Y_{2,lam} \cdot (3500 - Re_{LF}) + Y_{2,tur} \cdot (Re_{LF} - 2040)}{3500 - 2040}, \qquad [20]$$

where $Y_{2,lam}$ and $Y_{2,tur}$ are the values of Y_2 evaluated by assuming laminar and turbulent liquid film flow at the present Re_{LF}, respectively.

3. LIMIT OF THE POSSIBLE OPERATING CONDITIONS

3.1. Method to determine the limit conditions

It is clear from section 2.5 that [19] is an equation which is equivalent to the first equation of [1]. A standard method of obtaining the envelope of [1] is to solve the simultaneous equations [1] with two unknowns (e.g. Lee & Bankoff 1983). However, this is not necessarily an appropriate method under the involved conditions of two-phase flow, such as those in the present study, because of the difficulty of preparing the second equation of [1] and because of the difficulty of grasping the physical meaning. In the present study, therefore, a new method is developed to determine the envelope by pursuing the limit boundary for the existence of real roots of the first equation of [1] only.

As has been mentioned in section 2.5, if values of j_G^*, j_L^* and δ/R $(=Y_1)$ are assumed, the mangitude of Y_2 can be calculated; and figure 2 is a typical diagram resulting from such calculations. It is found in figure 2 that each intersection point between the Y_1- and Y_2-lines designates a set of real roots (j_G^*, j_L^* and δ/R) satisfying [19], and that if the gas flow rate is increased beyond $\sqrt{j_G^*} = 0.490$, no real roots can appear. In other words, the contact point between the Y_1- and Y_2-lines at $\sqrt{j_G^*} = 0.490$ is the limit condition of the possible gas flow rate under the present conditions of $D = 50$ mm and $\sqrt{j_L^*} = 0.5$.

Figure 3 is a diagram showing a process to determine the contact point, in such situations, by computer. First, under a fixed condition of $\sqrt{j_L^*}$, a sequential computation of Y_2 starts from certain small values of j_G^* and δ/R (point A). During the initial stage where the value of Y_2 is lower than that of $Y_1 (=\delta/R)$, the magnitude of j_G^* is increased in a stepwise manner so as to move the Y_2-point (represented by ●) successively in the direction of B until the Y_2-point exceeds the Y_1-line.

The computation now enters the second stage, where the magnitude of Y_2 is calculated, increasing δ/R in a stepwise manner under a fixed condition of j_G^*, when the Y_2-point moves successively along

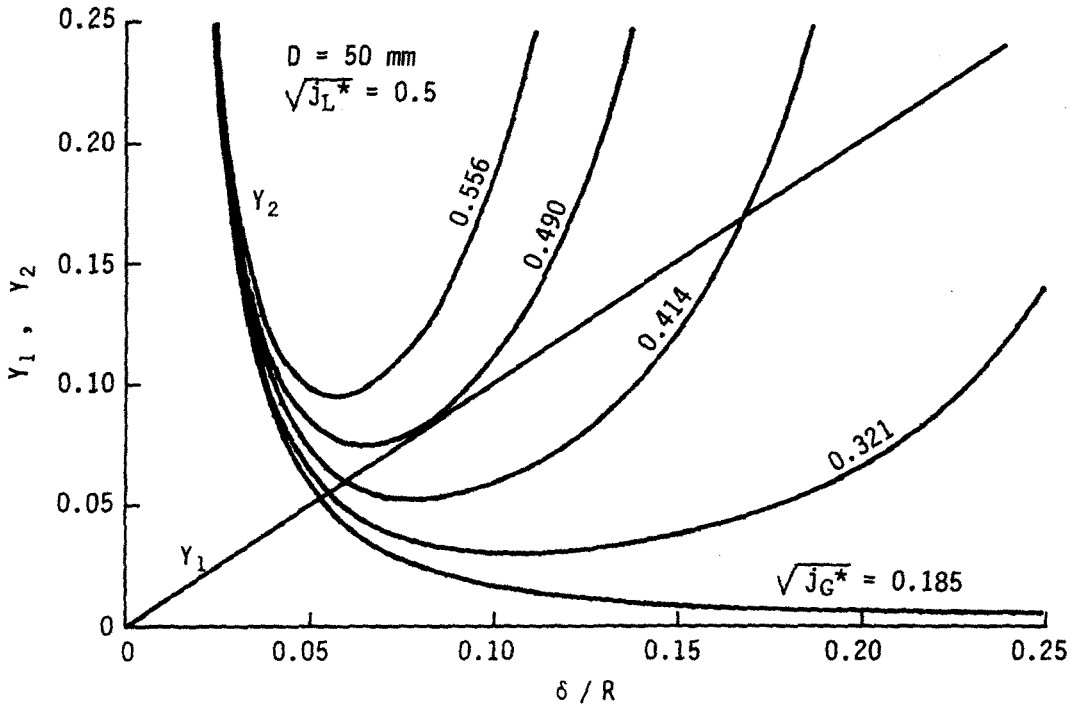

Figure 2. Variations of Y_1 and Y_2 with liquid film thickness δ/R (air–water, 101.3 kPa, 20°C).

a curved line (like the C-line, for example). Moving along such a line, the Y_2-point soon goes down below the Y_1-line; the same computation procedure as above is repeated by increasing the fixed value of j_G^* little-by-little until the final situation of the D-line is reached. During the computation,

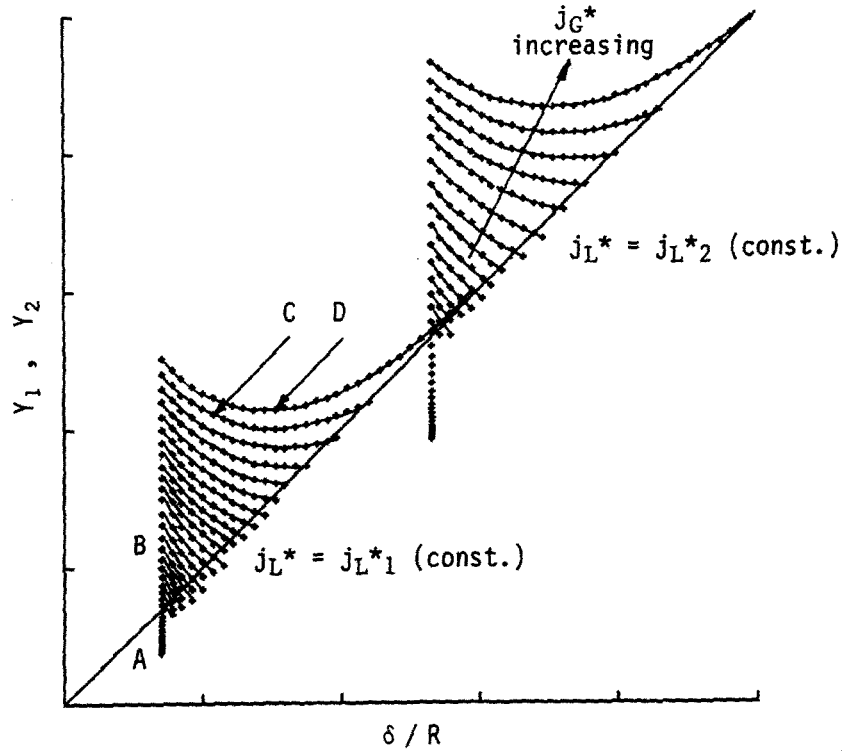

Figure 3. Method to determine the contact point between the Y_1- and Y_2-lines.

this final situation can be readily detected by the appearance of a state wherein the Y_2-point is above the Y_1-line and the gradient between the adjacent two Y_2-points exceeds 45°. Then, if the increment of j_G^* between the C- and D-lines is sufficiently small, the limit condition can be determined accurately by averaging the respective states at the right ends of the C- and D-lines. The envelope in figure 1 is an example obtained by such a procedure.

3.2. Generation of the limit conditions

The concept of the envelope of [1], or that of figure 1, is liable to give the impression that the limit condition is generated through the variation of flow situations corresponding to the change in the respective cross-sectional areas of the two-phase flow or the change in the void fraction ϵ (or δ/R). In fact, according to the author's previous study (Katto 1992), it is probable that this situation actually appears in a very special case of vertical annuli with extremely thin clearances.

In the present flow, however, the change in the void fraction ϵ (or δ/R) can affect not only the cross-sectional areas but also the interfacial shear stress when the core gas flow is in the turbulent or transition region (see [17]). Therefore, there is an interesting problem as to which of the two effects mentioned above is more important for the generation of the limit conditions.

It is obvious from figure 2 that the limit conditions appear only when the Y_2–δ/R curve is downwardly convex. Y_2, which represents the right-hand side of [6] or [7], can be divided into two parts: the first term relating to factors of the liquid film flow such as Γ or τ_w; and the second term relating to the interfacial shear stress τ_i. Figure 4 presents the values of the first and second terms of Y_2 vs δ/R, under the same conditions as those of figure 2, and shows that the first term decreases monotonously with increasing δ/R, while the second term increases very rapidly with δ/R when the gas flow rate is sufficiently high. (*Note:* the mangitude of Re'_G ranges from 9700 to 17,400 for the line of $\sqrt{j_G^*} = 0.321$, for example.) It is then readily proved that this special character of the second term of Y_2 is caused by the second term on the right-hand side of the C_{fi} correlation [17], and that its effect on τ_i is rapidly accelerated by the increase in the gas flow rate: $(u')^2$ (see [15]).

Accordingly, it can be concluded that the limit conditions in the present model are generated through the characteristics of the interfacial shear stress τ_i, which increases with the liquid film thickness δ/R. In connection with this problem, it may be of interest to note that the C_{fi} correlation of type [17] has played an important role in almost all the theoretical studies on the limit conditions

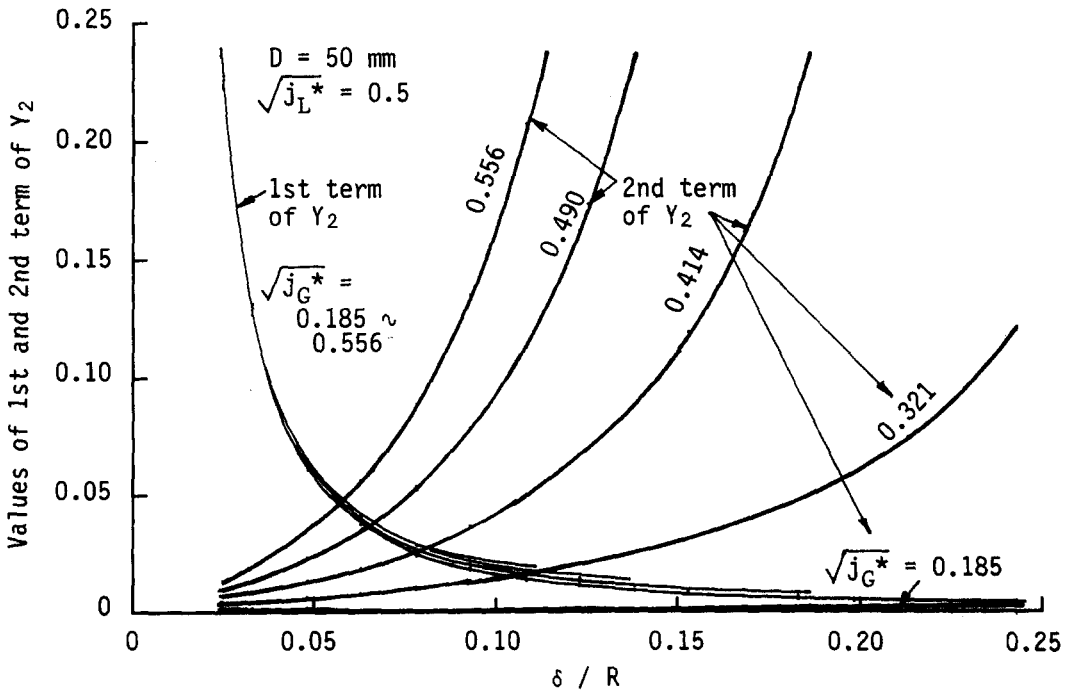

Figure 4. Variations of the values of the first and second term of Y_2 vs δ/R (air–water, 101.3 kPa, 20°C).

of countercurrent annular flow (Bharathan *et al.* 1979; Bharathan & Wallis 1983; Lee & Bankoff 1983; Dobran 1985; Reed & Tien 1987; Katto & Watanabe 1992).

3.3. The ϵ and non-ϵ models

The results of the preceding section suggests the possibility that, even if δ/R and $(\delta/R)^2$ are negligible compared with unity on the right-hand sides of [6] and [7] (which is equivalent to $\epsilon = 1$ except for the effect of δ/R on τ_i), the limit conditions still appear. In addition, the dashed lines in figures 5 and 6 shows that the magnitudes of δ/R and $2\tau_i/(\rho_L g R)$ at the limit conditions are considerably small compared with unity, particularly in the region of small magnitude of j_L^*.

Accordingly, let us assume $\delta/R \ll 1$ and $2\tau_i/(\rho_L g R) \ll 1$ in [6] and [7] together with an ordinary condition of $\rho_G/\rho_L \ll 1$, and the above two equations reduce to the following equations, respectively:

$$\frac{\delta}{R} = \frac{3\Gamma\mu_L}{\rho_L^2 g \delta^2 R} + \frac{3}{2}\frac{\tau_i}{\rho_L g R} \qquad [21]$$

and

$$\frac{\delta}{R} = \frac{\tau_w + \tau_i}{R\rho_L g}. \qquad [22]$$

In addition, [9], [10] and [12] also reduce to

$$u_G = \frac{m_G}{\rho_G \pi R^2}, \quad u_L = \frac{m_L}{\rho_L 2\pi R\delta} \quad \text{and} \quad \mathrm{Re}'_G = \frac{u'2R}{\nu_G}, \qquad [23]$$

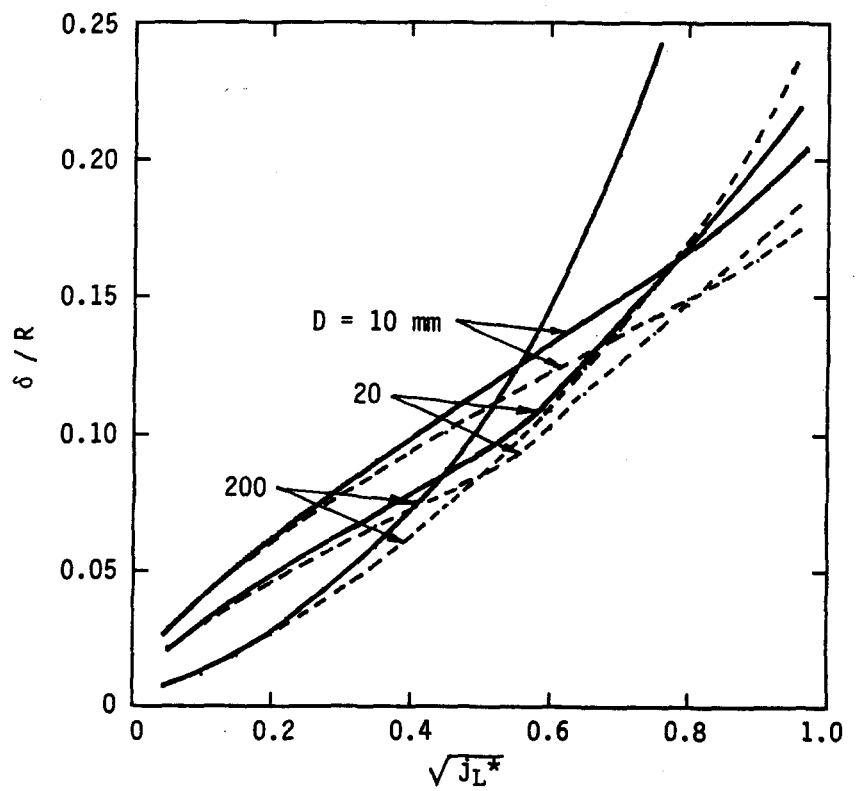

Figure 5. Magnitude of δ/R at the limit condition (air–water, 101.3 kPa, 20°C); ——, non-ϵ model; - - -, ϵ model.

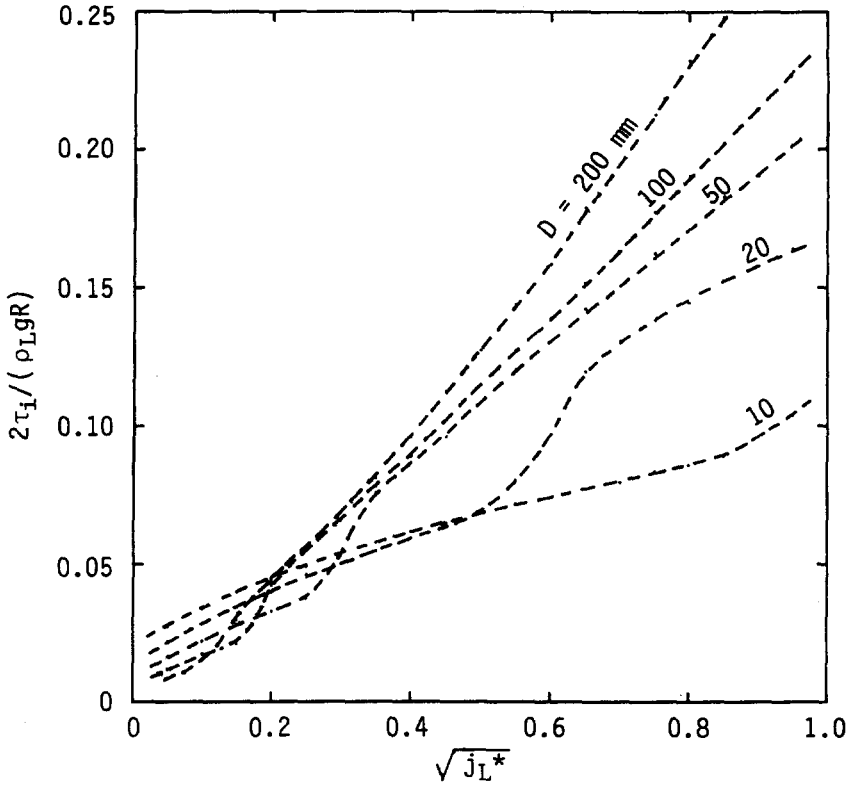

Figure 6. Magnitude of $2\tau_i/(\rho_L gR)$ at the limit condition (air–water, 101.3 kPa, 20°C); - - -, ϵ model.

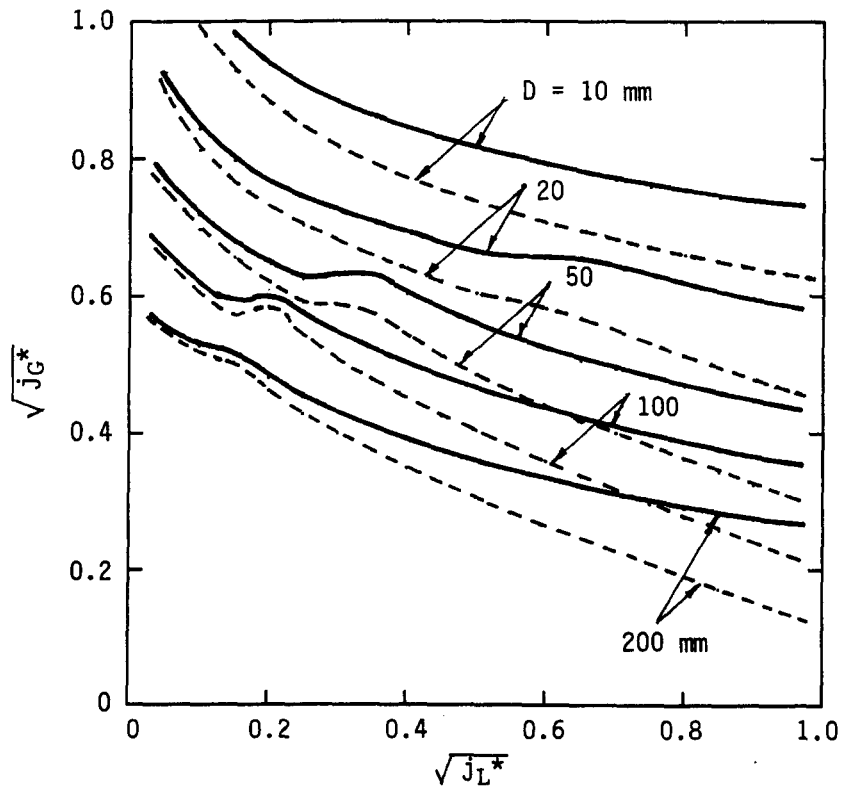

Figure 7. Flooding velocity (air–water, 101.3 kPa, 20°C); ——, non-ϵ model; - - -, ϵ model.

respectively. The above-mentioned [21]–[23] are the same equations as employed in a previous study (Katto & Watanabe 1992) analyzing the CHF of boiling in a bottom-closed vertical tube.

Let us designate the limit condition model based on [6] and [7] as the ϵ model, and that based on [21]–[23] as the non-ϵ model. The calculation procedure of Y_2 in the case of the non-ϵ model is listed in part (B) of table 1. Figure 7 presents the limit conditions predicted by the above-mentioned two models for the onset of flooding of an air–water system (101.3 kPa, 20°C). Figure 8 presents the Reynolds numbers of the gas and liquid flow at the limit conditions of figure 7, respectively. In figure 8, the relationship between Re_{LF} and $\sqrt{j_L^*}$ is presented by the solid lines only, because [13] and [14] are commonly used to evaluate Re_{LF} for the two models. Meanwhile, figure 5 presents the magnitude of the dimensionless liquid film thickness δ/R at the limit conditions of figure 7. It is noticed from these figures that the difference between the two models is not so great particularly in the region of, say, $\sqrt{j_L^*} < 0.4$.

4. COMPARISON WITH THE EXPERIMENTAL DATA FOR THE ONSET OF FLOODING

As has already been mentioned, flooding is a phenomenon with many complicated aspects. In addition to this, accurate detection of the onset of flooding is rather difficult, because of the abrupt change in the flow configurations near the onset of flooding. In fact, experimental results of flooding tend to differ according to the method of detection.

The limit conditions dealt with so far in this paper are those of steady-state countercurrent annular flow. Therefore, it is advisable to compare the prediction of the present analysis with the experimental data obtained for the onset of flooding in flow systems which are free, as far as possible, from unstable wave motion, such as a vertical tube with constructions to prevent the interaction between the downward flow of liquid and the converging flow of gas from the surrounding space near the bottom end of the tube.

The limit conditions predicted by the ϵ and non-ϵ models are then compared with the experiment data of Suzuki & Ueda (1977), in figure 9, and of Celata *et al.* (1991), in figure 10. In these experiments, a downwardly divergent duct was attached to the bottom end of the tube. A trend is noticed in these figures that the predictions agree with the data comparatively well in the region of, say, $\sqrt{j_L^*} < 0.4$, but the situation becomes rapidly worse if $\sqrt{j_L^*}$ is increased further. Perhaps, such an end structure as mentioned above may be insufficient to prevent the interaction of the two fluids at very high liquid flow rates.

In addition, figures 9 and 10 (together with other similar comparisons omitted here due to limited space) suggest a trend that the non-ϵ model performs better than the ϵ model regarding correspondence with the data. This is a strange result, but it may derive from the approximations in parts of the present analysis: wherein the independence of each phase is assumed according to the determination of the flow state by the Reynolds number; and the interaction between the two phases is 'hidden' in the assumption of the interfacial shear stress based on the interfacial-roughness (i.e. irregular deformation of the interface).

Figure 11 shows comparisons of the non-ϵ model prediction with the experimental data of Tien *et al.* (1989) for four different tube diameters. In this case, the predictions shows a rough trend to agree with the data points up to $\sqrt{j_L^*} = 1$, probably because of their experimental conditions that air is supplied to the test tube through a concentric tube of diameter smaller than that of the test tube to avoid the positive interaction of the liquid flow.

On the other hand, the data in figure 12 is that obtained by Tien *et al.* (1989) for sharp-ended tubes and, accordingly, it is a natural consequence that a noticeable deviation from the prediction is observed.

Finally, figure 13 presents the data obtained by Bharathan *et al.* (1979) for tubes rounded at both the top and bottom ends with radii greater than the tube diameter. In this case, a noticeable trend is that the data points appear with a linear relationship between $\sqrt{j_G^*}$ and $\sqrt{j_L^*}$ such as that of the well-known Wallis' correlation (Wallis 1961). However, good agreement is observed between the predicted and experimental results at very low values of $\sqrt{j_L^*}$. Perhaps, the interaction between

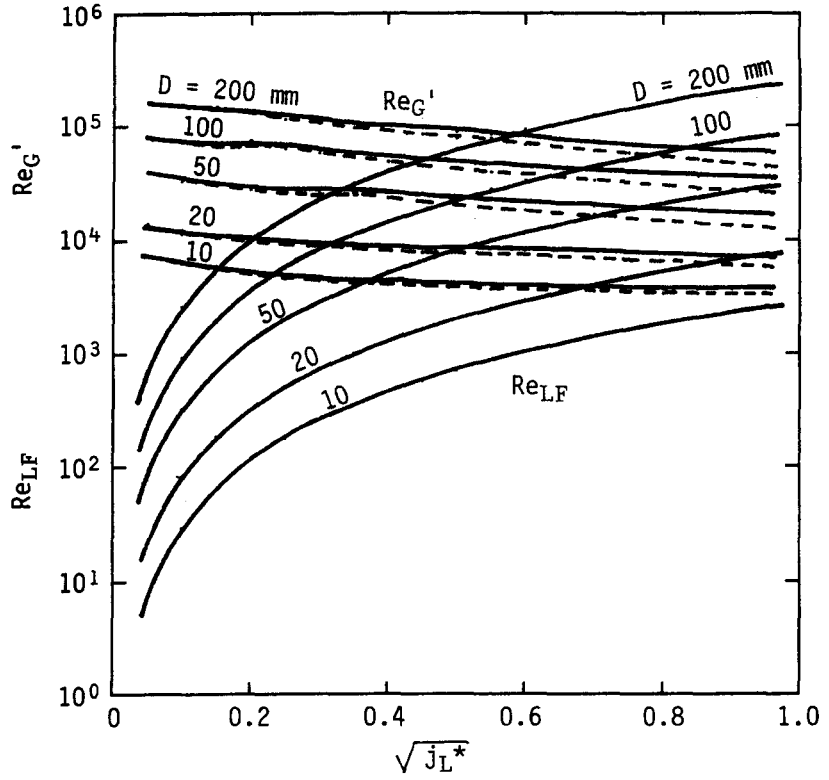

Figure 8. Reynolds numbers of core gas flow and liquid film flow (air–water, 101.3 kPa, 20°C); ——, non-ϵ model; - - -, ϵ model.

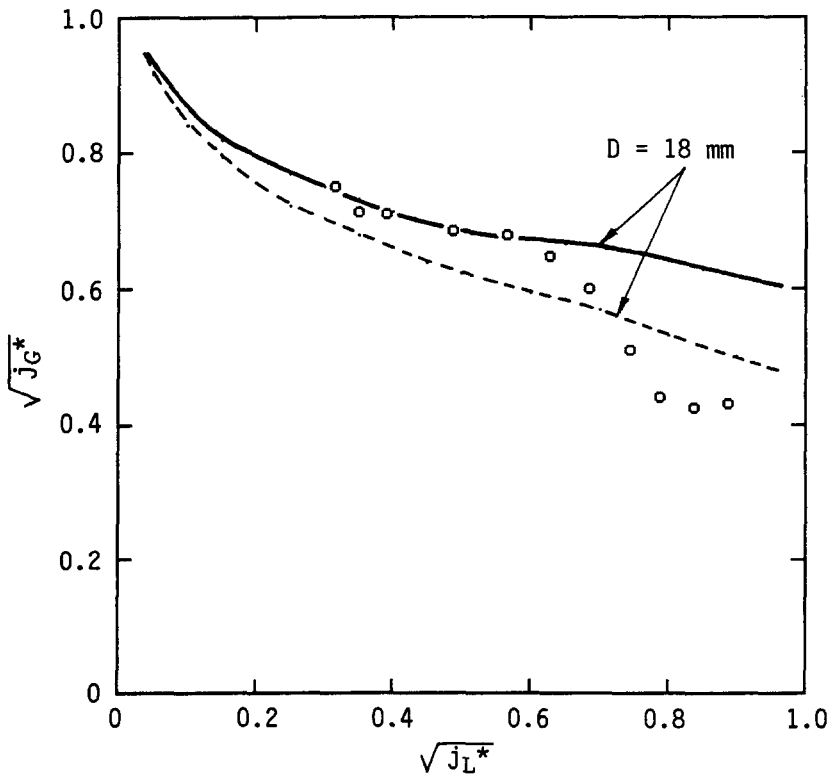

Figure 9. Comparison with flooding velocity data [Suzuki & Ueda (1977); air–water]; ——, non-ϵ model; - - -, ϵ model.

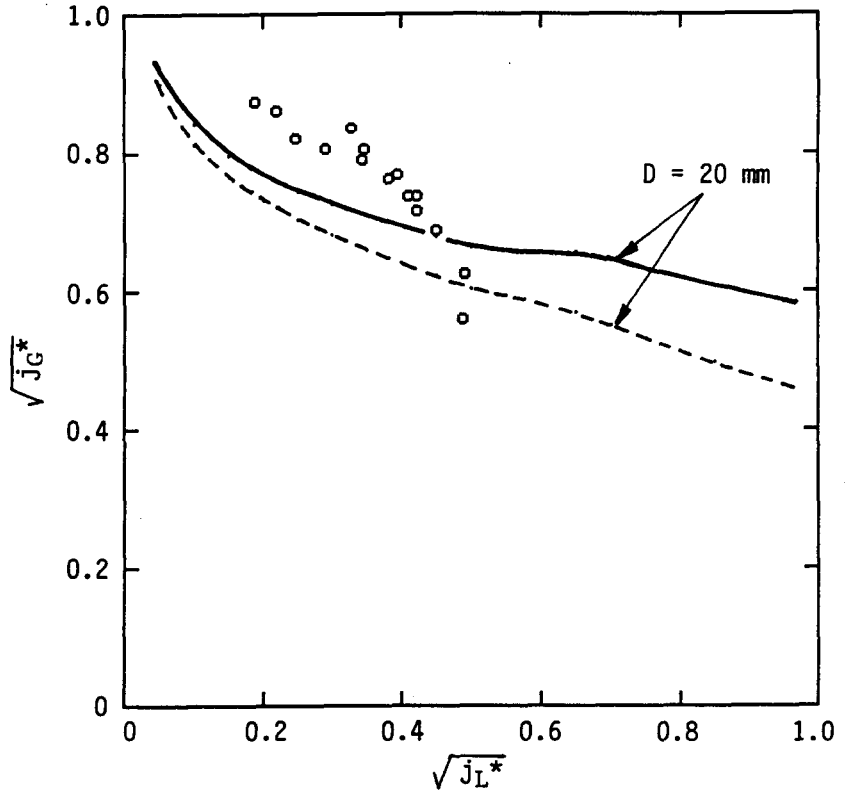

Figure 10. Comparison with flooding velocity data [Celata *et al.* (1991) air–water]; ——, non-ϵ model; - - -, ϵ model.

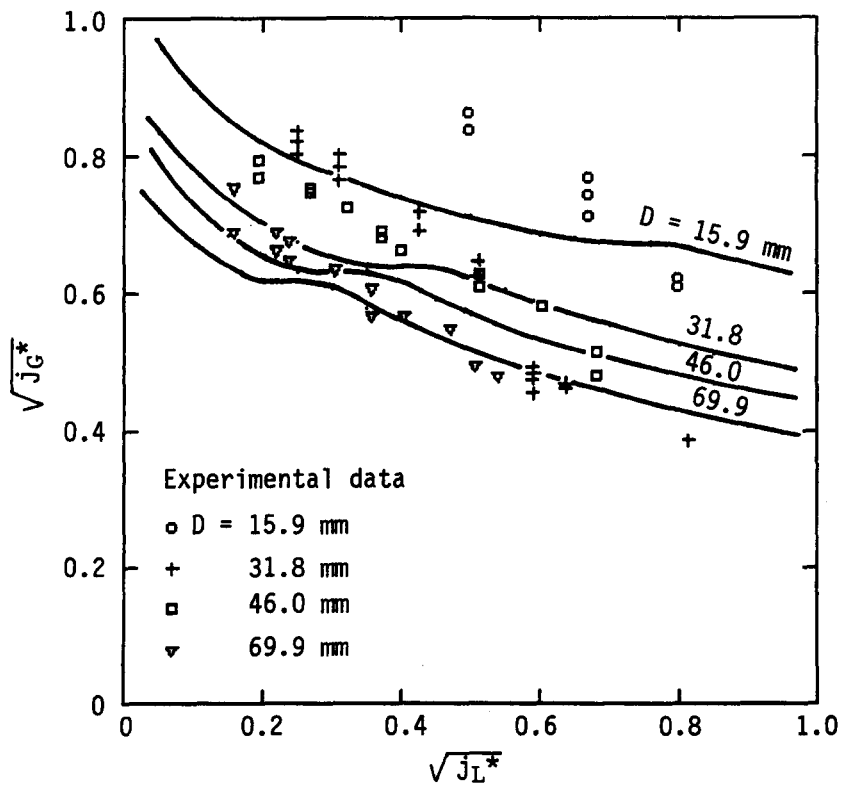

Figure 11. Comparison with flooding velocity data [Tien *et al.* (1989); air–water]; ——, non-ϵ model.

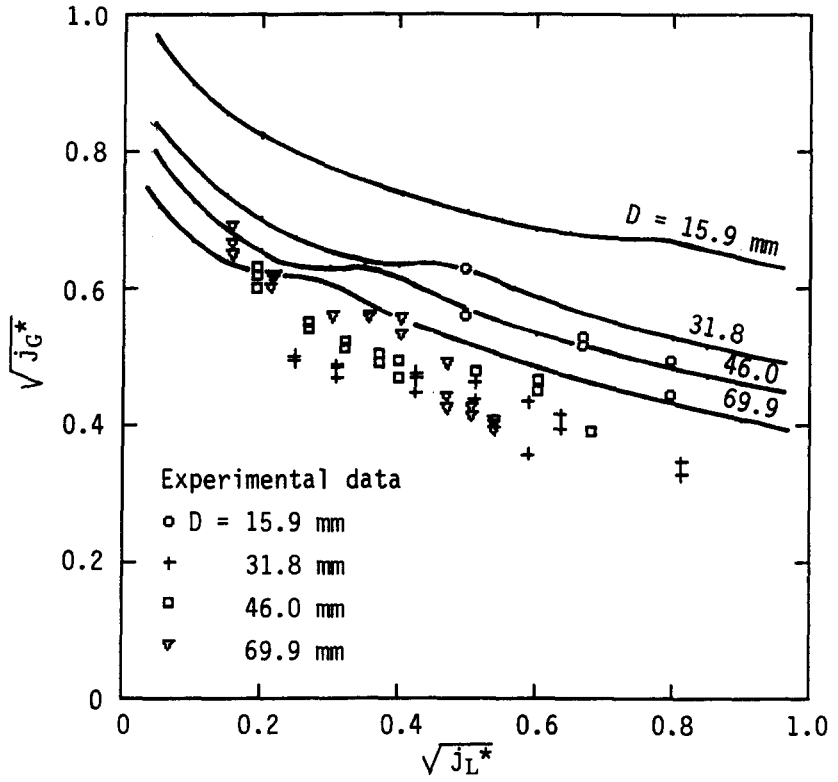

Figure 12. Comparison with flooding velocity data [Tien *et al.* (1989); air–water]; ——, non-ϵ model.

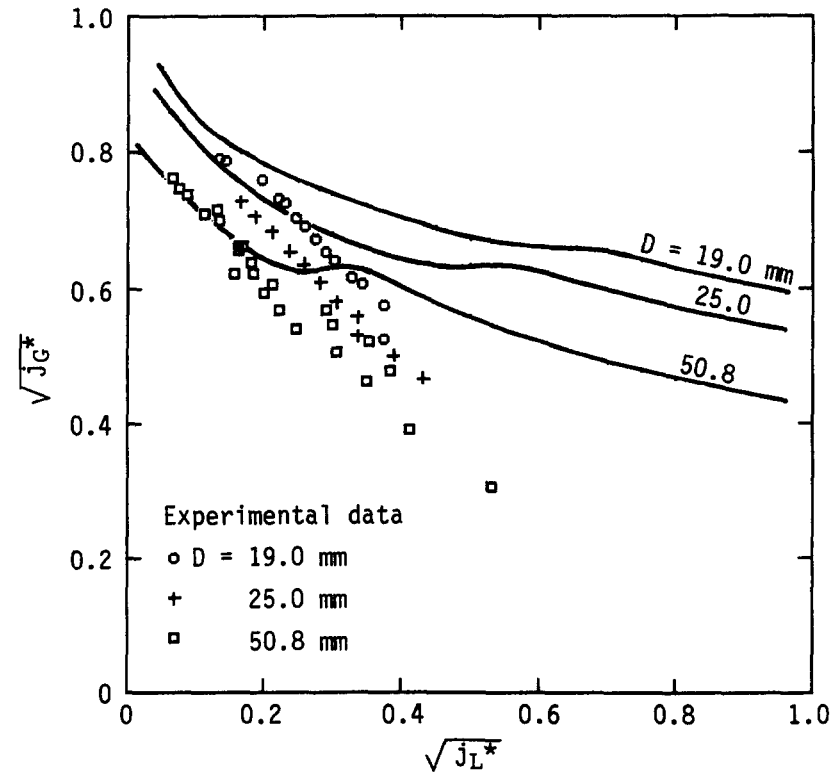

Figure 13. Comparison with flooding velocity data [Bharathan *et al.* (1979); air–water]; ——, non-ϵ model.

two phases may be avoided at the bottom end for this kind of tube only when the liquid film flow rate is extremely low.

5. COMPARISON WITH DATA FOR THE CHF OF BOILING IN BOTTOM-CLOSED TUBES

Detailed analysis of the CHF of boiling in bottom-closed vertical tubes is not the object of the present study, so figure 14 alone is shown here for reference. In this figure, the lines descending to the right represent the flooding curves predicted by the non-ϵ model for water, R-113 and R-22, under the conditions of diameter D and pressure p_1, p_2 and p_3 listed outside the figure. The straight lines passing through the origin represent the following relationship:

$$\sqrt{j_G^*} = \sqrt[4]{\frac{\rho_L}{\rho_G}} \cdot \sqrt{j_L^*}, \qquad [24]$$

which is derived from the mass balance of $m_G = m_L$ that holds in the present boiling system.

Therefore, the limit conditions of stable boiling should appear at the intersection points of the above-mentioned two lines obtained for each identical experimental condition; and it is of interest to note that these intersection points agree fairly well with the experimental CHF data [the data obtained by Katto & Hirao (1991) and Katto & Watanabe (1992) and unpublished data for R-113 and R-22 by Katto *et al.*]. Finally, figure 14 shows an important fact: in the CHF case the magnitude of $\sqrt{j_L^*}$ does not exceed 0.3, even for the R-22 experiments with every high vapor/liquid density ratios up to $\rho_G/\rho_L = 0.136$ (at $p_3 = 2808$ kPa).

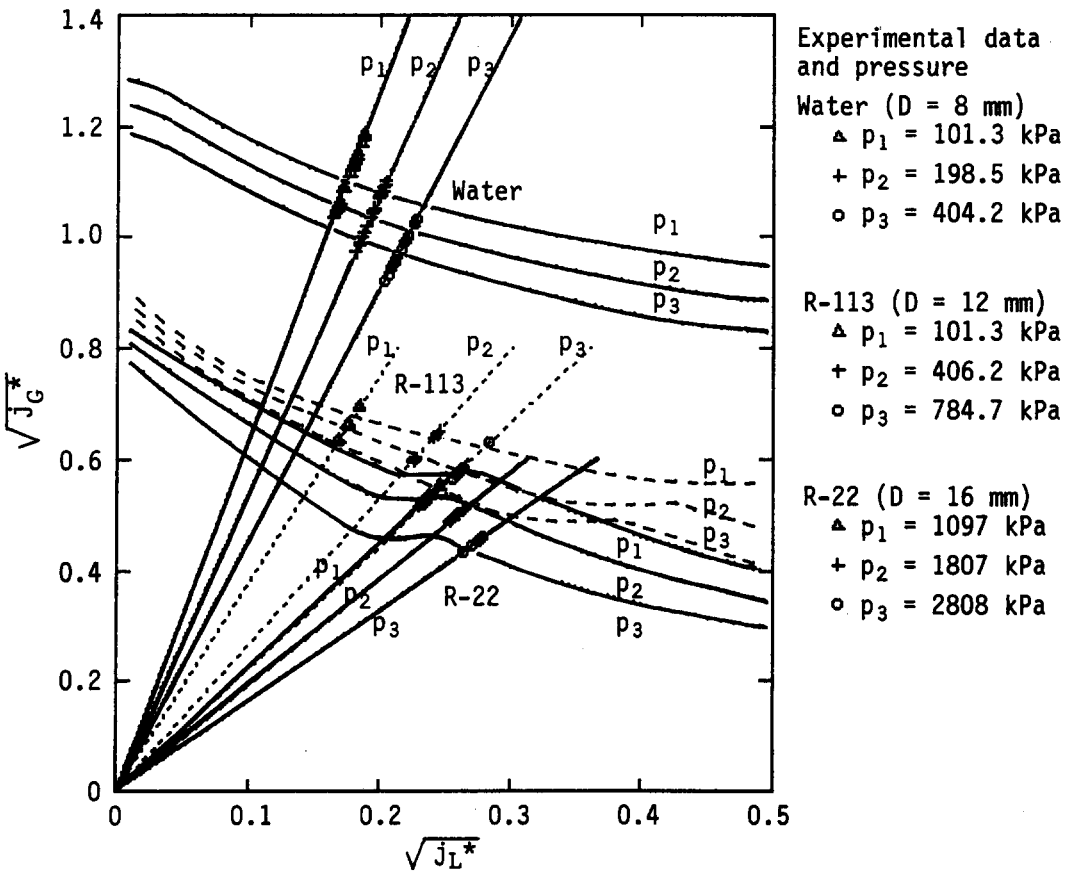

Figure 14. Comparison with CHF data of water, R-113 and R-22 boiling in bottom-closed vertical tubes.

6. CONCLUSIONS

(1) A study has been performed on the analysis of the limit conditions for steady-state countercurrent annular flow, developing a new method to determine the limit conditions by discriminating between the real and imaginary region as to the root of the flow equation [19].
(2) In the above-mentioned flow, the limit conditions appear only when the interfacial friction increases with the liquid film thickness. The change in the cross-sectional areas of the gas and liquid flow, due to the variation in the void fraction ϵ (or the dimensionless liquid film thickness δ/R), is not the main cause of the limit conditions.
(3) Two distinctive models, i.e. an ϵ model (which considers the full effects of the variation of the void fraction ϵ) and a non-ϵ model (which does not consider the effects of ϵ except for the effect on the interfacial friction) are dealt with. These two models do not differ very much with respect to the prediction of the limit conditions.
(4) However, when compared with the experimental data obtained for a vertical tube with a construction to prevent the interaction between the gas and liquid flow at the bottom end, it is found that the non-ϵ model performs better than the ϵ model with regard to the agreement with the experimental data. Roughly speaking, it is likely that the non-ϵ model applies fairly well to the prediction of flooding in the range of $\sqrt{j_L^*} = 0$ to 0.4.
(5) In the case of the CHF of saturated boiling in a bottom-closed vertical tube, the limit conditions appear under rather simple situations compared with flooding, and $\sqrt{j_L^*}$ does not exceed 0.3; accordingly, the non-ϵ model may probably be useful to predict the CHF.

REFERENCES

BANKOFF, S. G. & LEE, S. C. 1986 A critical review of the flooding literature. In *Multiphase Science and Technology* (Edited by HEWITT, G. F., DELHAYE, M. & ZUBER, N.), Vol. 2, pp. 95–180. Hemisphere, Washingon, DC.

BHARATHAN, D. & WALLIS, G. B. 1983 Air–water countercurrent annular flow. *Int. J. Multiphase Flow* **9,** 349–366.

BHARATHAN, D., WALLIS, G. B. & RICHTER, H. J. 1979 Air–water countercurrent annular flow in vertical tubes. EPRI Report NP-1165.

CELATA, G. P., CUMO, M., FARELLO, G. E. & SETARO, T. 1991 Hysteresis effect in flooding. *Int. J. Multiphase Flow* **17,** 283–289.

DOBRAN, F. 1985 Steady-state characteristic and stability thresholds of a closed two-phase thermosyphon. *Int. J. Heat Mass Transfer* **28,** 949–957.

IMURA, H., KUSUDA, H. & FUNATSU, S. 1977 Flooding velocity in a countercurrent annular two-phase flow. *Chem. Engng Sci.* **32,** 79–87.

KATTO, Y. 1992 Analytical study of critical heat flux of counter-flow boiling in a very thin, bottom-closed vertical annulus. In *Transport Phenomena Science and Technology 1992* (Edited by WANG, B.-X.), pp. 69–76. Higher Education Press, Beijing.

KATTO, Y. & HIRAO, T. 1991 Critical heat flux of counter-flow boiling in a uniformly heated vertical tube with a closed bottom. *Int. J. Heat Mass Transfer* **34,** 993–1001.

KATTO, Y. & WATANABE, K. 1992 An analytical study on the critical heat flux of countercurrent boiling in a vertical tube with a closed bottom. *Int. J. Heat Mass Transfer* **35,** 3021–3028.

LEE, S. C. & BANKOFF, S. G. 1983 Stability of steam–water countercurrent flow in an inclined channel: flooding. *Trans. ASME Jl Heat Transfer* **105,** 713–718.

MARON, D. M. & DUCKLER, A. E. 1984 Flooding and upward film flow in vertical tubes—II. Speculations on film flow mechanism. *Int. J. Multiphase Flow* **10,** 599–621.

MCQUILLAN, K. W. & WHALLEY, P. B. 1985 A comparison between flooding correlations and experimental flooding data for gas–liquid flow in vertical circular tubes. *Chem. Engng Sci.* **40,** 1425–1440.

REED, J. G. & TIEN, C. L. 1987 Modeling of the two-phase closed thermosyphon. *Trans. ASME Jl Heat Transfer* **109,** 722–730.

RICHTER, H. J. 1981 Flooding in tubes and annuli. *Int. J. Multiphase Flow* **7,** 647–658.

SUZUKI, S. & UEDA, T. 1977 Behaviour of liquid films and flooding in counter-current two-phase flow—Part 1. Flow in circular tubes. *Int. J. Multiphase Flow* **3,** 517–532.

TAITEL, Y., BARNEA, D. & DUCKLER, A. E. 1982 A film model for the prediction of flooding and flow reversal for gas–liquid flow in vertical tubes. *Int. J. Multiphase Flow* **8,** 1–10.

TIEN, C. L. & LIU, C. P. 1979 Survey on vertical two-phase countercurrent flooding. EPRI Report NP-984.

TIEN, C. L., CHUNG, K. S. & LIU, C. P. 1979 Floding in two-phase countercurrent flows. EPRI Report NP-1283.

WALLIS, G. B. 1961 Flooding velocities for air and water in vertical tubes. UKAEA Report AEEW-R123.

WALLIS, G. B. 1969 *One-dimensional Two-phase Flow.* McGraw-Hill, New York.

WALLIS, G. B. 1970 Annular two-phase flow, Part 1: a simple theory. *Trans. ASME Jl Bas. Engng* **92,** 59–72.

WHALLEY, P. B. 1987 *Boiling, Condensation, and Gas–Liquid Flow*, p. 31. Clarendon Press, Oxford.